Journal of Forestry Research (2026) 37:164
https://doi.org/10.1007/s11676-026-02104-0

ORIGINAL PAPER

Central Himalayan tree-ring density network reveals warm-season temperature variability back to 1775 CE

Tim Nahtz[1] · Frederick Reinig[1] · Max C. A. Torbenson[1,2] · Inga K. Homfeld[1] · Philipp Römer[1] · Eileen S. Kuhl[3] · Marcel Kunz[1] · Antonia Kölzer[1] · Sugam Aryal[4] · Achim Bräuning[4] · Narayan P. Gaire[5] · Ulf Büntgen[2,6,7] · Jan Esper[1,2]

Received: 1 October 2025 / Accepted: 10 June 2026

Abstract Although recognized as Asia's "Water Tower", our understanding of past natural and recent anthropogenic enforced climate change is limited for much of the Himalayas. The main contributing factors for that are sparse and short meteorological observations, seasonally restricted and often imprecise proxy archives, and spatially heterogeneous and temporally unstable climate dynamics. Here we present a network of five maximum latewood density (MXD) chronologies from 135 living fir (*Abies spectabilis*) trees from sites near the upper treeline between 3220 and 3750 m a.s.l. in Nepal. Individual series were processed to preserve interannual, decadal, and centennial-scale variability. The resulting composite chronology was calibrated against April–September (AMJJAS) temperatures over the period 1951–2022 CE ($r_s = 0.64$; $p < 0.001$), enabling the first MXD network-based temperature reconstruction for the Central Himalayas. Despite the relatively short reconstruction coverage (1775–2022 CE), it by far surpasses any regional instrumental record and explains more than 40% of AMJJAS temperature variance over much of the Asian Water Tower during the calibration period (1951 – 2022 CE). This novel high-resolution insight reveals the coldest period following the 1815 Tambora eruption, with the strongest summer cooling found in 1817 rather than 1816 CE (– 1.6 °C relative to 1951–1980 CE). Our results demonstrate that MXD is a robust proxy for warm-season temperatures in monsoon-influenced regions, capturing a strong and widespread signal across South and Southeast Asia, and holds great potential for further spatio-temporal extension of the MXD network.

Keywords Dendroclimatology · Temperature reconstruction · Temperature variability · Central Himalaya

Project funding: This work was supported by the German Research Foundation (Grant No. 514551733), the ERC Advanced Grant (# 882727; Monostar),the Czech Science Foundation grant HYDRO8 (23–08049S), TU-NPAR-079/80-ERG-12, the co-funded EU project AdAgriF (#CZ.02.01.01/00/22_008/0004635), and the ERC Synergy Grant (# 101118880; Synergy-Plague).

The online version is available at http://link.springer.com.

Corresponding editor: Lei Yu.

Supplementary Information The online version contains supplementary material available at https://doi.org/10.1007/s11676-026-02104-0.

✉ Tim Nahtz
nahtz@geo.uni-mainz.de

[1] Department of Geography, Johannes Gutenberg-University Mainz, Mainz, Germany

[2] Global Change Research Institute of the Czech Academy of Sciences, Brno, Czech Republic

[3] Deutscher Wetterdienst, Offenbach, Germany

[4] Department of Geography, Friedrich-Alexander-University Erlangen-Nuremberg, Erlangen, Germany

[5] Department of Environmental Science, Patan Multiple Campus, Tribhuvan University, Lalitpur, Nepal

[6] Department of Geography, University of Cambridge, Cambridge, UK

[7] Department of Geography, Faculty of Science, Masaryk University, Brno, Czech Republic

Published online: 15 July 2026

Introduction

The Himalayas, often referred to as the "Water Tower of Asia" (Xu et al. 2009) or the "Third Pole" (Qiu 2008), are a vital water source for hundreds of millions of people (Nie et al. 2021; Xu et al. 2009; ICIMOD 2023) across Asia. The region is recognized as a climate change hotspot (Diffenbaugh & Giorgi 2012), with a warming rate well above the global average (Xu et al. 2009). Between 1951 and 2014, the Himalayas warmed by about 1.3 °C (Krishnan & Dhara 2020), with an accelerating trend towards the present, exceeding 0.2 °C per decade (Duan & Xiao 2015). Warming rates are even greater at higher elevations, reaching up to 0.4 °C per decade at 3500–4000 m a.s.l. (Palazzi et al. 2017; Pepin et al. 2015; Ren et al. 2017; Thakuri et al. 2019). This elevation-dependent warming contributes to widespread glacier retreat, with potentially severe implications for the inhabitants of hydrologically connected lowland areas, disrupting future water supply. (Dussaillant et al. 2024; ICIMOD 2023; Sigdel et al. 2020; Wang et al. 2015).

Understanding past climate variability is therefore essential for contextualizing these recent warming trends. However, reliable instrumental records are sparse in the Central Himalayas often starting only in the mid-twentieth century, and remain unevenly distributed across the region's complex topography (Shrestha et al. 1999; DHM 2017). Proxy records are the only means to extend knowledge about past climate variability beyond the observational record. Multi-proxy reconstructions, including tree rings, ice cores, and historical documents, have demonstrated their value by highlighting that the twentieth century was the warmest period in Asia over the past millennium (PAGES 2k Consortium 2013; Shi et al. 2015). Tree rings stand out among these proxies, as they provide an annual to sub-annual resolution and absolute dating accuracy.

In the Nepalese Himalayas, encompassing much of the Central Himalayan mountain range, high-resolution climate reconstructions have relied primarily on tree-ring records. Dendrochronological studies in the greater region have shown that tree-ring width (TRW) can be sensitive to pre-monsoon and spring temperatures (e.g., Aryal et al. 2020; Cook et al. 2003; Thapa et al. 2015), to previous winter temperatures (e.g., Gaire et al. 2020), or to drought and precipitation (e.g., Bhandari et al. 2019; Gaire et al. 2017 2019; Panthi et al. 2017). However, significant relationships between tree growth and warm-season or late summer temperatures, which coincide with the monsoon season (DHM 2017), are only sparsely observed. As a result, only a few high-resolution reconstructions in Nepal for these seasons exist (e.g., Cook et al. 2013; Gaire et al. 2023). Across the broader Himalayan-Karakoram-Tibetan Plateau region, summer and warm-season temperature reconstructions are mainly based on tree-ring density, especially maximum latewood density (MXD). In comparison to TRW, MXD reflects summer temperature signals to a greater degree (Esper et al. 2015), making it the ideal parameter to overcome the lack of past temperature information not encompassed in TRW measurements. Such MXD chronologies have been developed for the western Indian Himalaya (e.g., Pant et al. 2000), the Karakoram (e.g., Hughes 2001; Khan et al. 2024), and the Tibetan Plateau (e.g., Bräuning & Mantwill 2004; Duan et al. 2019; Huang et al. 2025; Li et al. 2017, 2018, 2015; Liang et al. 2016; Nie et al. 2023; Wang et al. 2010). In the Central Himalaya, however, only one density-based warm-season temperature reconstruction (Sano et al. 2005; end year 2000 CE) and one sensitivity study (Bräuning 2003; end year 1998 CE) exist, both from western Nepal. Respectively, neither record includes the most recent two decades, thus not capturing the elevating warming trend across the Himalayas (Hamal et al. 2021; Krishnan et al. 2019).

Here, we introduce the first network-based MXD reconstruction of warm-season temperatures from the Central Himalaya, using high-elevation *Abies spectabilis* sites near the tree line. Our record untangles the impact of recent climate warming on regional tree growth up to 2022 CE Furthermore, extending back to the eighteenth century, this record provides crucial high-resolution insights into regional climate variability over the past ~ 250 years.

Materials and methods

Tree ring data and sampling sites

Tree-ring data from five *Abies spectabilis* sites located between 3220 and 3750 m a.s.l. in the Central Himalayas (Fig. 1) are analyzed. They cover a longitudinal range from 82.0°E to 86.1°E and latitudes between 28.1°N and 29.5°N, extending from eastern to western Nepal. The sites Ghorepani (Ghore) and Kalinchowk (Kalin) were sampled in the late 1970s (Schweingruber 2002a, 2002b) and obtained from the International Tree Ring Data Bank (ITRDB; Guiterman et al. 2024). Jumla site was sampled in the late 1990s (Bräuning 2003) and the remaining two sites, Rara and Cholangpati (Chola), were newly established for this study.

Here, 50 mixed-aged trees were sampled in spring and fall 2023 CE, with two cores extracted at breast height, making 2022 the final complete ring. TRW was measured using a LINTAB system with a precision of 0.01 mm, and crossdating accuracy was controlled using the COFECHA program (Holmes 1983). MXD was measured using a WALESCH densitometer following standard protocols (Björklund et al. 2019; Schweingruber et al. 1978) at the Johannes Gutenberg University Mainz, Germany, and the Swiss Federal Research Institute (WSL) in Birmensdorf, Switzerland.

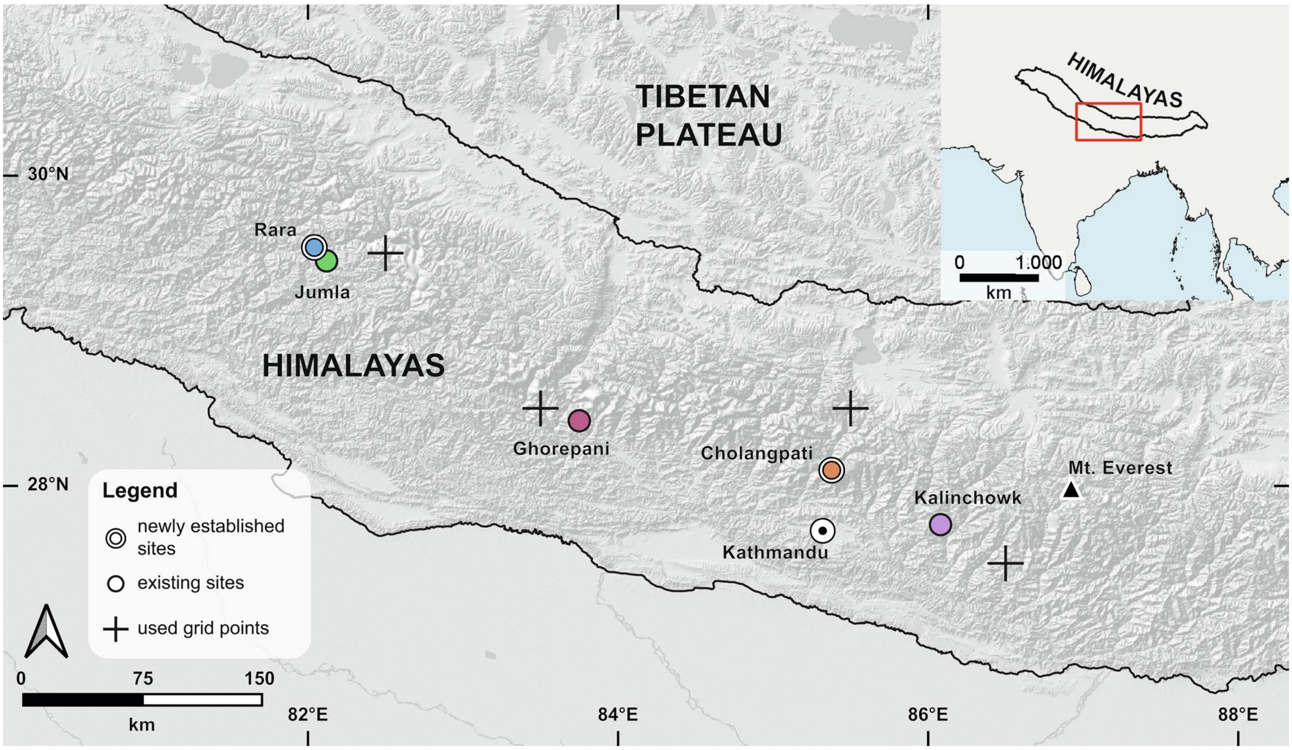

Fig. 1 Map of site locations within the Himalayas (Liu & Zhu 2022). Black crosses represent used temperature grid points from Berkeley Earth 1° gridded temperature data (Berkeley Earth 2025a)

Detrending and chronology building

To remove biological age trends, all series were detrended using a negative exponential curve (NegEx) or linear regression to calculate ratios in the program ARSTAN v41d (Cook 1985; Cook & Kairiukstis 1990; Cook & Krusic 2020). For each site, all cross-dated samples considering a COFECHA score $r > 0.2$ were entered into a site chronology. To ensure a comparable sample structure across sites, only series longer than 100 years were included (90 years for Chola; Fig. 2). The variance of site chronologies was stabilized by first calculating residuals between the chronologies and a 31-year centered Gaussian-weighted moving average. These were then divided by a 101-year centered moving standard deviation, scaled to match the mean and standard deviation of the original residuals, and finally added back to the 31-year filter. Composite chronologies representing different combinations of the sampling locations were built by truncating each site chronology at a replication of five series and then averaging the resulting chronologies. A threshold of 0.8 for the expressed population signal (EPS) was applied to define a reliable period of the chronologies. The climate signal was tested for means of three, four, and five sites.

Regional Curve Standardization (RCS) was applied to preserve additional low-frequency climate signals (Briffa et al. 1992a, b). As RCS requires an extensive range of sample ages (Esper et al. 2002), all samples that surpassed the site chronology screening were included, regardless of previous length restraints. The series were pruned to a cambial age range from 30 to 100 years (Fig. S1), and series shorter than ten years were excluded (Homfeld et al. 2024). All resulting series were RCS detrended using ratios and averaged to produce a regional chronology, which was variance-stabilized as described above.

After scaling to instrumental temperatures (see below), the low-frequency climate signal was emphasized by applying a 101-year Gaussian-weighted low-pass filter. To capture high-frequency variations, the residuals between the same 101-year Gaussian filter and a NegEx detrended composite chronology were calculated. Those residuals were then added to the smoothed low-frequency signal of the RCS chronology. This combined approach allows the preservation of long-term trends, which are likely better captured by RCS, while retaining high-frequency variability from the NegEx detrending (Cook et al. 2003).

Climate data and signal assessment

For each site, monthly mean temperatures (T_{mean}) were extracted for the closest grid point (Fig. 1) of the most recent Berkeley Earth Surface Temperature Dataset (BEST) (Berkeley Earth 2025a; Rohde & Hausfather 2020). The

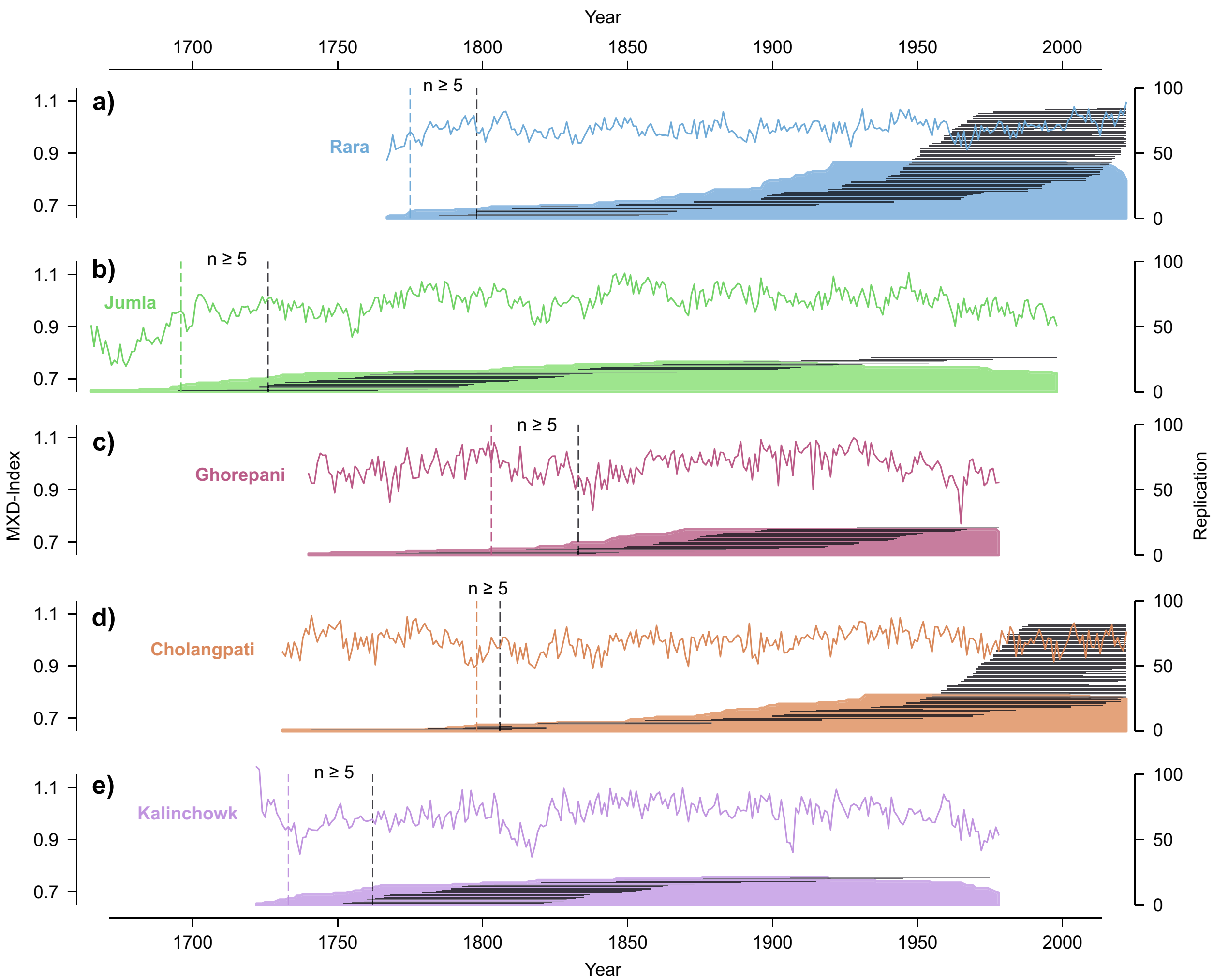

Fig. 2 Negative exponential (NegEx) detrended MXD-chronologies for the five sites (from west/top to east/bottom). Colored lines show the standardized chronologies along with their replication. Black bars indicate the pruned series used for RCS detrending

longest common period without missing values across all grid points, 1870 to 2022 CE, was used for climate correlations. For the combined chronologies, temperature data from the grid points closest to the included sites were averaged. The grid points used in the analysis have an average elevation of 4230, 4587, 3116, and 2563 m a.s.l. from west to east.

Both temperature and tree ring data were tested for normality using the Lilliefors test (Lilliefors 1967) before calculating bootstrapped Spearman correlations between the chronologies and monthly and seasonally averaged climate data. This was done for the periods 1870–1950 CE and 1951–end of the corresponding chronology to assess climate-growth relationships and specify a target season. Stationarity was tested using 31-year running correlations and significances determined using a studentized permutation test (Yu & Hutson 2024). To account for high autocorrelation, permutations were performed using a block resampling scheme. Fisher's z-transformation test was used to assess the significance of differences between correlations (Fisher 1921).

The composite chronology with the strongest climate-growth relationship was calibrated against the corresponding averaged temperature data using simple linear regression over three periods (full 1951–1975 CE, early: 1951–1986 CE, late: 1976–2022 CE). These periods were selected to ensure that the gridded data were based on observations from Nepal (Berkeley Earth 2025b; Shrestha et al. 1999). Model performance was evaluated using the reduction of error (RE) and coefficient of efficiency (CE) statistics in a split calibration approach, where values greater than 0 indicate predictive skill (Cook et al. 1994). To assess potential diverging trends between MXD and temperature data, the Durbin-Watson (DW) statistic was calculated over the 1951–2022 CE calibration period, as well as within 31-year moving windows over the complete overlapping period (1870–2022 CE). The DW tests for autocorrelation in proxy-target residuals, with values around 2 indicating insignificant trends (Durbin & Watson 1971; Wilson et al. 2007). For final reconstruction, the regressed MXD data were scaled to match the mean and standard deviation of the 1900–1990 CE temperature data (Esper et al. 2005). Reconstruction uncertainties were estimated using the prediction interval (Olive 2007), and the long-term trend was assessed using a modified Mann–Kendall test (Hamed & Rao 1998; Hussain & Mahmud 2019).

Results

The single-site chronologies span the period 1665–2022 CE, with the Jumla site providing the longest record, covering 1665–1998 CE, and the Ghore site the shortest, starting in 1740 and ending in 1978 CE Between 20 (Ghore) and 43 (Rara) MXD series are averaged per site. The shortest mean segment length (MSL) is 152 years at Ghore and the longest 232 years at Jumla. Mean maximum latewood density varies across sites, from 0.70 g/cm^3 at Kalin to 0.83 g/cm^3 at Rara (Fig. S2a, Tab. 1). First-order autocorrelation is highest at Jumla (0.61) and lowest at Chola (0.25). The interseries correlations (rbar) range from 0.37 in Rara to 0.51 in Kalin (Tab. 1). Results from the Lilliefors tests indicate that MXD values in all site chronologies except Chola are normally distributed. Inter-site correlations range from $r_s = 0.18$ between Rara and Ghore to $r_s = 0.51$ between Kalin and Jumla (Fig. S2b). Correlations based on first differences are consistently higher, ranging from 0.24 between Rara and Kalin to 0.63 between the Ghore and Chola sites (all $p < 0.05$). The correlations between each site chronology and the mean of the other sites remain stable over time (Fig. S3). The composite chronologies consist of 135 series for the mean-of-five sites covering 1696 to 2022 CE, 115 series for the mean-of-four sites from 1733 to 2022 CE, excluding the Ghore site, and 92 series for the mean-of-three sites from 1775 to 2022 CE, with both the Ghore and Jumla sites removed. According to the EPS values, the mean-of-four and mean-of-five chronologies fall below the 0.8 threshold at the beginning of the 1750s, whereas the mean-of-three chronology exceeds this threshold from the 1790s onward (see Fig. S4).

Climate correlations

The climate-growth analysis across the sites revealed slight regional differences with regard to the monthly temperature responses. During the 1951–2022 CE calibration period, spring and late summer temperatures show the most dominant impact on tree growth, indicated by the highest monthly correlations in April, August, and September across the MXD sites (Fig. 3b). The strongest significant single-month correlations are found in August for Rara ($r_s = 0.65$; $p < 0.001$), Chola ($r_s = 0.27$; $p < 0.05$), and Kalin ($r_s = 0.40$; $p < 0.01$), and in March for Jumla ($r_s = 0.29$; $p < 0.05$; Fig. 4 and Figs. S5, S6, S7, S8 and S9). For Ghore, no significant correlation is detected. During the earlier 1870–1950 CE period, April and August temperatures show the strongest relationship across the sites, with a focus on April in four of the five sites (Fig. 3a). Correlations range from $r_s = 0.23$ ($p < 0.05$) at Rara to $r_s = 0.58$ ($p < 0.001$) at Kalin. Only Chola shows the strongest response to August temperatures ($r_s = 0.28$, $p < 0.001$), but it also correlates with April at $r_s = 0.24$ ($p < 0.05$). Intersite covariance and correlation with April–September growing season temperatures are relatively stable until the late 1930s, but thereafter break down in Ghore. From the late 1970s onward, the correlations at Jumla and Chola decline, reaching $r_s = 0$; but only Chola recovers after the late 1980s (Fig. 3c, d).

The three-site, four-site and five-site composite chronologies show strongest correlations with April, July, August, and September temperatures and the April-September seasonal mean (Fig. 4a). Correlations for April range from $r_s = 0.40$ to 0.45 ($p < 0.01$), for July from $r_s = 0.40$ to 0.46 ($p < 0.01$), for August from $r_s = 0.60$ to 0.63 ($p < 0.001$) and for September from $r_s = 0.47$ to 0.52 ($p < 0.01$). Seasonal correlations for April-September vary between $r_s = 0.61$ and 0.64 ($p < 0.001$), with the highest correlation observed for the four-site composite ($r_s = 0.64$; $p < 0.001$). A decline in correlation is seen in May and June across all composites, followed by an increase in

Table 1 MXD site chronology characteristics (MSL = mean segment length, Rbar = interseries correlation, Ac1 = autocorrelation (lag -1); 1926–1975 = common period of all MXD Abies datasets from Europe and Asia available on ITRDB)

Site	Lat	Lon	Elevation (m a.s.l.)	Period	Radii	MSL	Mean max. densities	Rbar	Ac1 (n ≥ 5)	Ac1 (1926–1975)
Rara	29.54	82.04	3600	1767–2022	43	154	0.83	0.36	0.48	0.50
Jumla	29.45	82.12	3500	1665–1998	23	232	0.71	0.45	0.61	0.36
Ghorepani (Ghore)	28.42	83.75	3220	1740–1978	20	152	0.75	0.48	0.43	0.06
Cholangpati (Chola)	28.10	85.38	3750	1731–2022	28	153	0.80	0.41	0.25	0.56
Kalinchowk (Kalin)	27.75	86.08	3720	1722–1978	21	201	0.70	0.51	0.57	0.53

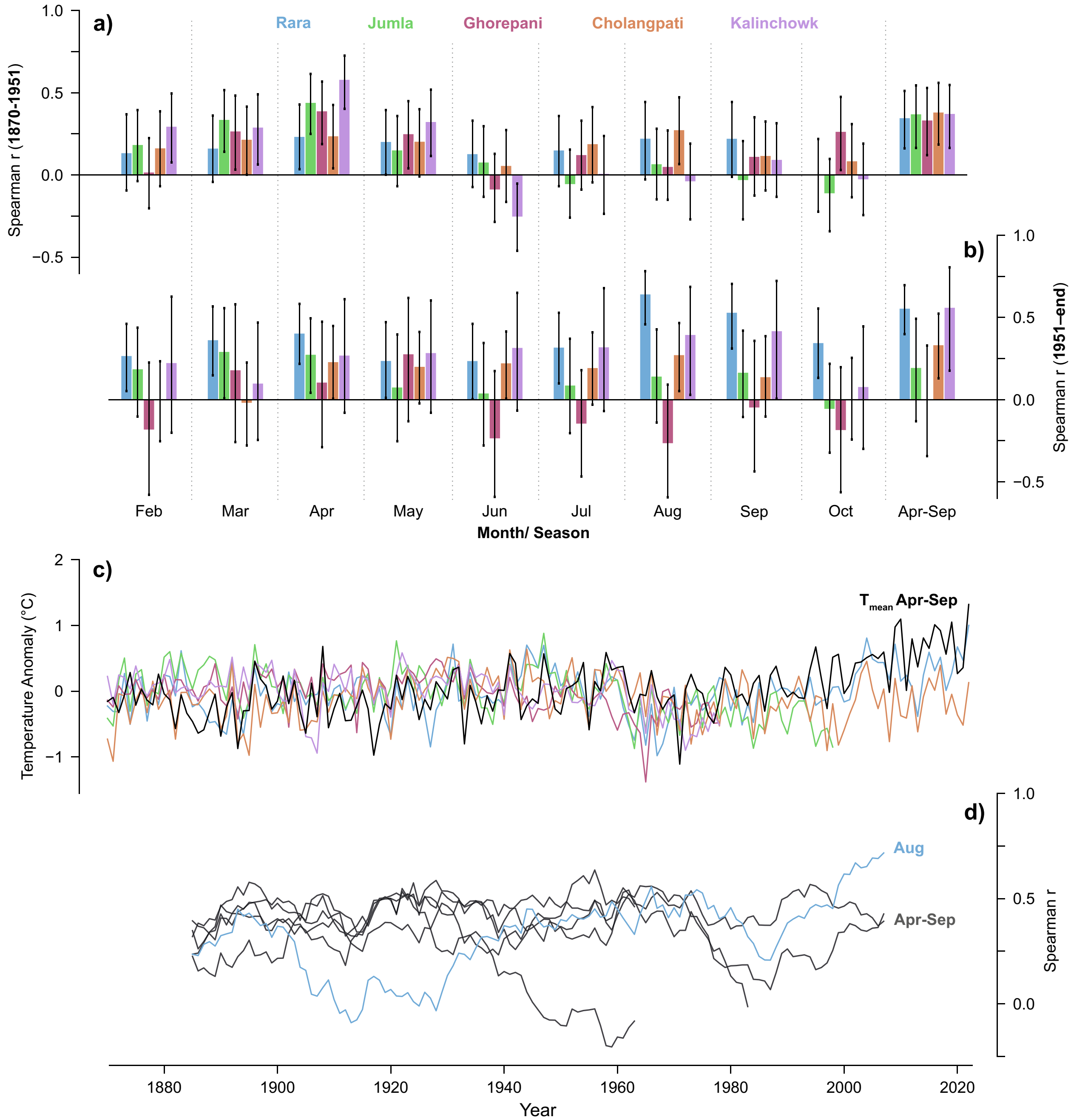

Fig. 3 **a** Spearman correlations between site chronologies and monthly/ seasonal mean temperatures for the period 1870–1950 CE; **b** same as **a** but for the period 1951–2022 CE; **c** single site chronologies scaled to Apr – Sep T_{mean} for the 1900–1990 period; **d** 31-year centered running correlations between site-chronologies and Apr – Sep T_{mean} (black lines) over the period 1870–2022 CE The strongest single-site correlation observed for Rara in August in blue

July. Running correlations for April-September remain temporally stable, except for a dip from the mid- to late-1980s, which is slightly less pronounced in the three site composites (Fig. 4b). The strongest spatial correlations are found in central Nepal extending at $r_s > 0.5$ across the southern Tibetan Plateau, Bhutan, Bangladesh, and parts of India and Myanmar (Fig. 5a). Correlations based on first differences are generally weaker (maximum $r_s = 0.51$), covering similar regions but with a less extensive reach. Moderate negative correlations ($r_s \geq -0.33$) can be found in the Tajikistan–Uzbekistan region (Fig. 5b).

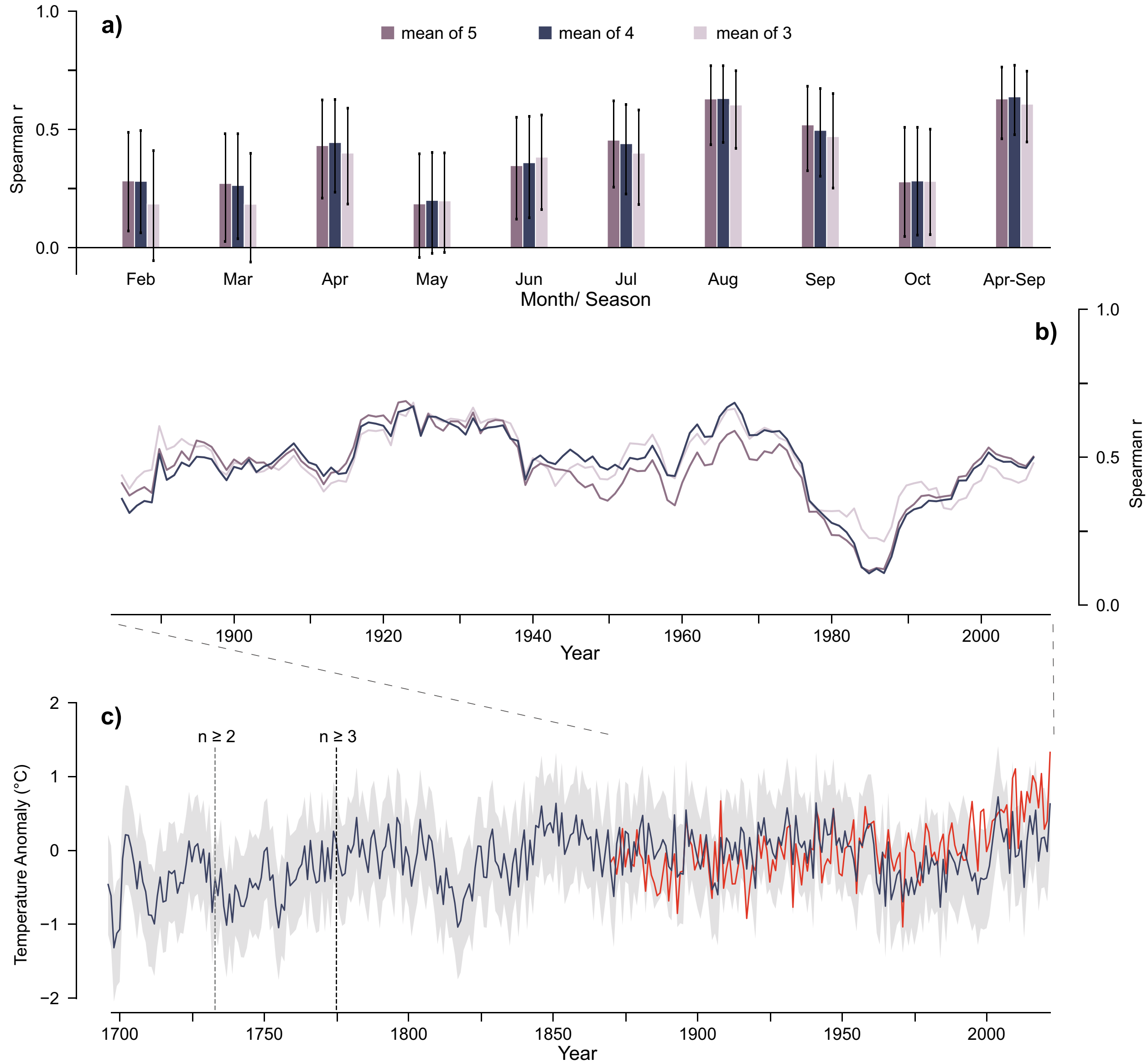

Fig. 4 **a** Spearman correlation between composite chronologies and monthly/seasonal T_{mean} for the period 1951–2022 CE; **b** 31-year centered running correlations between composite chronologies and Apr – Sep T_{mean} over the period 1870–2022 CE; **c** Reconstructed Apr – Sep T_{mean} based on the mean-of-four composite chronology (dark blue); grey shading represents the prediction interval (90th percentile), red Berkeley T_{mean} Apr – Sep; dashed grey and black lines indicate replication of at least two and three chronologies

Calibration and transfer

The simple linear regression model for the whole calibration period (1951–2022 CE; Fig. S10) using the four-site composite chronology explains 40% of the variance of April-September mean temperatures. When applying a split-period calibration with the calibration period divided exactly in half, CE values become negative, indicating reduced predictive skill. Therefore, split calibrations were performed for the periods 1951–1975 and 1976–2022. Calibrating on the first period (1951–1975) explains 42% of the variance during the calibration and 35% of the variance during verification. The corresponding verification statistics indicate moderate predictive skill (RE = 0.40, CE = 0.08). Using the second calibration period window (1976–2022), the model explains 37% of the variance during the calibration and 39% during verification periods. Verification statistics are comparable to the first approach (RE = 0.48, CE = 0.04; Tab. 2). To further assess model stability, a leave-one-out calibration was performed. The resulting predictions closely match the full calibration, indicating consistent model behavior (Fig. S 11). The DW statistic for the full calibration period (DW = 1.42, $p < 0.01$) indicates positive autocorrelation in the residuals between the reconstructed and instrumental data. A

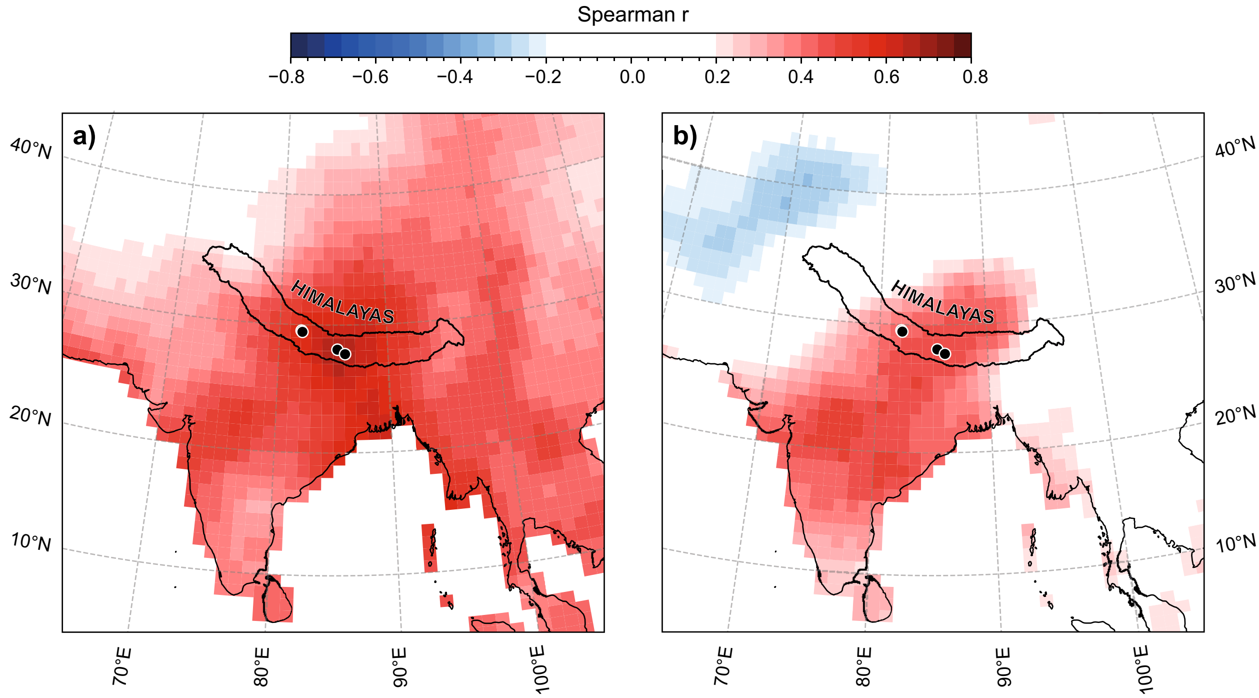

Fig. 5 **a** Spatial Spearman correlations between Apr–Sep T_{mean} (1951–2022 CE) and the mean-of-four composite chronology; b) spatial Spearman correlations based on first differences. Black dots represent the locations of the sites included in the mean-of-four chronology within the Himalayan Region (Liu & Zhu 2022)

Table 2 Calibration statistics for Apr–Sep T_{mean} reconstruction (CRE = calibration reduction of error, CE coefficient of efficiency, RE = reduction of error

Period	Calibration	Verification			
	r^2	CRE	r^2	RE	CE
1951–2022	0.40	0.40	–	–	–
1951–1975	0.42	0.42	0.35	0.40	0.08
1976–2022	0.37	0.37	0.39	0.48	0.04

declining trend in the running DW values outlines the presence of an increasing diverging trend between temperature and the MXD-chronology (Fig. S12).

Discussion

The dataset presented in this study is the largest density-based network for the Central Himalaya to date. High covariance between the single sites and consistent running correlations between the individual and the mean of the remaining sites (Fig. S3) suggest a coherent signal across the region, suitable for a climate reconstruction. The observed differences in raw mean MXD values among sites may result from a combination of factors, including measurements conducted in different laboratories (Mainz and WSL Birmensdorf) as well as variations in elevation and MSL, with younger rings usually showing higher MXD (Björklund et al. 2019). Nonetheless, these variations appear minor considering the displayed moderate to high correlations between the sites, also regarding their spatial distribution across Nepal (Fig. 1; Fig. S2b).

Climate correlations

The observed site-specific MXD responses to temperature provide novel insight into the complex regional climate growth relationships. At the single-site level, Rara exhibits the strongest correlation with August T_{mean}, which is consistent with the only other existing MXD-based reconstruction from Nepal (Sano et al. 2005). Rara appears to track recent warming reasonably well, whereas Chola, the second newly established site for this study, deviates from the recent temperature increase. The Ghore site, which lies furthest below the treeline, does not display significant temperature correlations during the calibration period. Studies by Hartl et al (2022) and Klippel et al (2020) have shown that the temperature sensitivity of MXD can weaken with decreasing elevation. We therefore interpret that the MXD at the Ghore site is not sharing the temperature limiting conditions at the higher-elevation sites, which is why it was excluded from the final reconstruction. As Ghore is situated in an area with one of the highest yearly precipitation rates in Nepal (DHM

2017), we assume that the MXD at this site is not moisture limited either, due to missing and reliable long-term instrumental data, we cannot state this for certain.

The composite chronologies generally exhibit a stronger climate signal than the individual sites (except for August correlations at Rara), as averaging reduces non-climatic noise and emphasizes the common climate signal, similar to standardizing series into a single chronology (Cook & Kairiukstis 1990). Since Ghore was excluded, and the average of the remaining four sites showed the strongest climate correlation among the composite chronologies (Fig. 4a), the four-site chronology was selected for the final reconstruction. April-September was chosen as the target season displaying the strongest overall climate-growth relationship.

April T_{mean}-MXD correlations are consistent with findings by Björklund et al. (2017) for the Northern Hemisphere and Hughes (2001) for the Karakoram, who report that spring conditions influence latewood density characteristics. This aligns with Rathgeber (2017), who suggests that carbon assimilated during the early growing season is used for cell-wall thickening in the latewood (Rathgeber 2017). Stronger correlations in April and late summer (August and September), compared to weaker signals in May and June, are in line with other density-based studies from neighboring regions, such as the Tibetan Plateau (Fan et al. 2009; Li et al. 2017 2018; Nie et al. 2023) and the Karakoram (Hughes 2001). The highest correlations between MXD and T_{mean} in August and September are in agreement with both the only other density-based Nepal dataset (Sano et al. 2005) and numerous studies from the Tibetan Plateau (Bräuning 2006; Bräuning & Mantwill 2004; Duan et al. 2019; Fan et al. 2009; Li et al. 2018, 2015; Nie et al. 2023; Wang et al. 2010; Xing et al. 2014) as well as from the Karakoram (Hughes 2001; Khan et al. 2024). This agrees with the understanding that late summer temperatures are particularly important for cell wall thickening (Cuny et al. 2019) and thus for latewood density, which is directly affected by cell wall dimensions (Björklund et al. 2017).

Most of the above-mentioned studies used August–September as the target season for temperature reconstructions. As in this study, the strongest climate-growth correlations are found for April-September (consistent with Fan et al. 2009; Hughes 2001), it was chosen as the target season. A slightly longer window, March-September, was used for the Western Nepal density reconstruction by Sano et al (2005). Additionally, several studies have focused on reconstructing summer minimum temperatures for the Tibetan Plateau (Huang et al. 2025; Liang et al. 2008, 2016).

Comparisons with other available temperature reconstructions reveal significant correlations with the averaged closest grid points of Cook et al. (2013) East Asian spatial temperature reconstruction ($r_s = 0.29$, $p < 0.001$), the February–June reconstruction for Nepal by Cook et al. (2003) ($r_s = 0.24$; $p < 0.01$) and the recently published August–September minimum temperature reconstruction for the Tibetan Plateau ($r_s = 0.24$, $p < 0.01$; Huang et al. 2025). In contrast, the reconstruction shows no significant correlation with a $\delta^{18}O$-based ice-core temperature reconstruction from the Nepal-China border ($r_s = 0.02$, $p = 0.41$; Thompson et al. 2000) or with a TRW-based summer temperature reconstruction from the Bhutanese Himalayas (Krusic et al. 2015; $r_s = 0.02$, $p = 0.54$). Beyond these statistical relationships, our reconstruction exhibits similar decadal-scale variability to the records mentioned above. All reconstructions identify the early nineteenth century as a pronounced cold period, with the 1810s representing one of the coldest decades of the past 250 years in the broader region (Fig. S13). A second shared cold phase can be identified in the 1960s and 1970s, although this decline is less striking in the Tibetan Plateau reconstruction (Huang et al. 2025) and the glacier-based record (Thompson et al. 2000). In contrast, warm periods are less clearly synchronized across the datasets, potentially reflecting a combination of differences in regional climate, varying seasonal sensitivities and temperature parameters reconstructed. However, the general presence of coherent cold phases, together with the moderate but significant correlations, indicates, that our reconstruction captures a common regional climate signal.

As shown in Fig. 4, running correlations between Apr – Sep T_{mean} and MXD remain relatively stable over time, except for a notable drop around 1984. This decrease is likely due to opposing effects of cold spring temperatures and slightly above average summer temperatures, which offset each other in the seasonal average (Fig. S14a). When only August–September is considered, this decline disappears (Fig. S14b).

While some single month running correlations show an increase towards the present (Fig. S15), diverging trends between the mean-of-four MXD reconstruction and warm-season temperatures can be observed. To identify the seasonality of this divergence, the mean-of-four reconstruction was scaled to the single-month temperatures and residuals between MXD and instrumental data are calculated (Fig. S16), revealing that the strongest declining trend can be observed at the beginning and the end of the target season (April and September).

Since only two sites cover the most recent 25 years and the Rara chronology tracks the current warming reasonably well (Fig. 3c), the described divergence is likely driven by Chola, which exhibits a weaker response to the recent temperature increase as described above. As Chola generally shows a weaker temperature-growth relationship than Rara, one possible explanation for the diverging trends may lie in differences in precipitation regimes between the two sites and between western and eastern Nepal in general. Western Nepal is more strongly influenced by westerlies during the winter, whereas eastern Nepal is more strongly influenced by the monsoon (DHM 2017). Chola might therefore be more sensitive to hydroclimatic conditions than Rara. However, due to the absence of publicly available high-resolution precipitation data, which would be essential to test this in such complex terrain, it cannot be assessed reliably. Additional explanations could involve microsite-specific factors that may have led to the diverging trends. As detailed ecological information about the stand is not available, any assumptions to that end would be speculative.

Preservation of low-frequency trends

No statistically significant low-frequency trend ($p = 0.30$) is present in the reconstruction (1775–2022 CE; Fig. 4c), indicating its limited potential to reflect multidecadal to centennial temperature fluctuations. This is also reflected in the low CE values, indicating a mismatch between the long-term trend in the instrumental data and the reconstruction during the calibration period, and is further supported by declining DW values toward the present. However, the reconstruction is robust in the high-frequency domain of the signal, underlined by the strong correlations between the temperature target and the reconstruction. To address the issue of missing low frequency, an approach originally introduced by Cook et al. (2003) for a Nepalese ring-width-based reconstruction was applied. The approach merges frequency-specific chronologies, here, the high-frequency component from the NegEx-detrended chronology, with the low-frequency signal from the RCS-detrended chronology (Fig. 6a, b). Moving away from the traditionally used even-aged datasets to mixed age classes (Nehrbass-Ahles et al. 2014), together with pruning, enables the use of RCS detrending on a living-tree dataset, to better preserve long-term trends (Esper et al. 2003; Homfeld et al. 2024). This approach results in a combined chronology that tracks the instrumental temperature more closely, especially in recent years, as shown by higher DW values in the calibration period (Fig. 6c, Fig. S12). The combined RCS-NegEx reconstruction underestimates April-September mean temperatures by 0.12 °C on average during the calibration period and by 0.13 °C in the earlier period, whereas the NegEx reconstruction underestimates the instrumental record by 0.33 °C during the calibration period and overestimates it by 0.19 °C in the earlier period (Fig. 6d). Additionally, the combined chronology explains more variance during the calibration period (45%) than the classic NegEx detrended chronology (Fig. S17). This improvement is also reflected in notably higher calibration statistics for the combined reconstruction, indicating higher predictive skill. For the early calibration period, CE and RE increase to 0.27 and 0.51, while for the later period they rise to 0.30 and 0.62 (Table S1).

In contrast to the NegEx-based reconstruction, the combined RCS-NegEx chronology exhibits a significant warming trend ($p < 0.001$), which aligns more closely with other reconstructions, such as the $\delta^{18}O$ glacier record from Thompson et al. (2000) and the MXD-based summer minimum temperature reconstruction by Huang et al. (2025; Fig. 7a). The combined RCS-NegEx chronology also reveals higher correlations with the glacier record ($r_s = 0.34$, $p < 0.001$) and with Huang et al. ($r_s = 0.54$, $p < 0.001$), compared to the NegEx reconstruction. The same applies for the Cook et al. (2013) spatial record ($r_s = 0.37$, $p < 0.001$). Only correlations with the frequency-combined reconstruction by Cook et al. (2003) are lower compared to the NegEx reconstruction $r_s = 0.04$ ($p = 0.31$). Overall, these results suggest an improved representation of both instrumental temperatures and broader regional temperature trends in the combined reconstruction, compared to the NegEx reconstruction.

1816: the year without a summer?

Five of the ten coldest years in the combined reconstruction occur between 1816 and 1820 CE, making the 1810s the coldest decade in the record. This period coincides with the aftermath of the 1815 CE Tambora eruption, the largest volcanic eruption in recorded history (Oppenheimer 2003), which was followed by a widespread temperature decrease across much of the Northern Hemisphere. In many European and North American records, 1816 CE appears as the coldest year of the past 250 + years and is widely known as the "Year Without a Summer" (Harington 1992; Luterbacher & Pfister 2015; Oppenheimer 2003; Pfister & White 2018). In this study, however, in contrast to many other Northern Hemisphere density records (e.g., Briffa et al. 1992b; Büntgen et al. 2006; D'Arrigo et al. 2006; Esper et al. 2025; Schneider et al. 2015; Wilson et al. 2016), 1817 CE appears to be the coldest year of the reconstructions (− 1.6 °C relative to 1951–1980 CE), followed by 1818 CE as the second coldest year. This discrepancy suggests that regional climate anomalies following major eruptions may not always align with hemispheric means.

One potential explanation lies in the structure of the density data. Parts of the dataset display unusually high lag-1 autocorrelation (Tab.1): Rara (Ac1 = 0.48), Jumla (Ac1 = 0.61), and Kalin (Ac1 = 0.57), along with the NegEx chronology (Ac1 = 0.53) and the combined reconstruction (Ac1 = 0.69). These values are significantly ($p < 0.01$) higher than the mean autocorrelation in MXD values of eleven millennium-length northern hemispheric chronologies described by Esper et al (2015; Ac1 = 0.17 for Hugershoff detrended and AC1 = 0.39 for RCS detrended) and could indicate a stronger memory effect in the climate signal, which is more typical of ring width data (Esper et al. 2015). However, when comparing the mean lag-1 autocorrelation

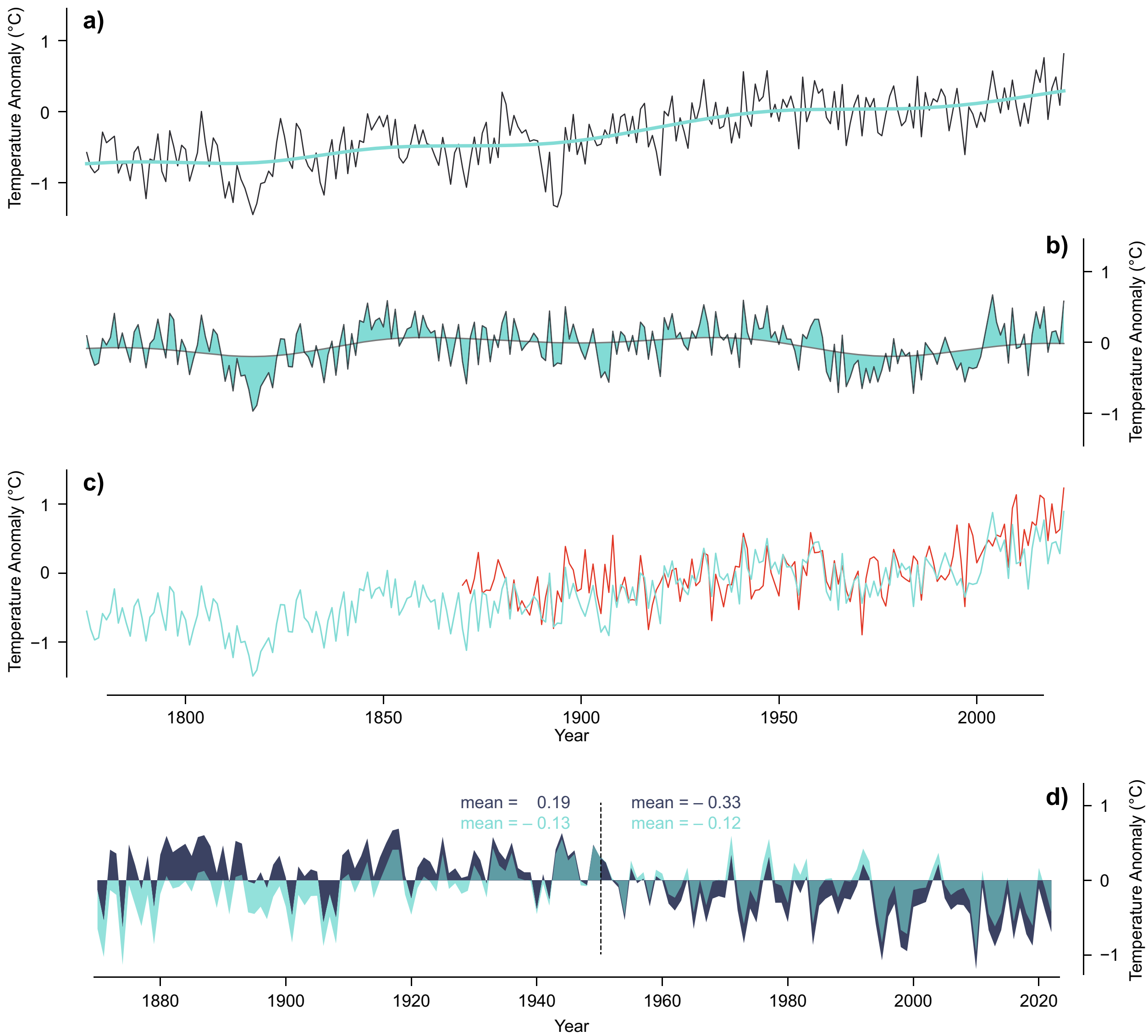

Fig. 6 **a** RCS-detrended chronology with 101-year Gaussian filter (turquoise); **b** NegEx-detrended mean-of-four chronology with residuals (turquoise) between the chronology and the 101-year Gaussian filter; **c** Combined chronology (turquoise), integrating the Gaussian filter from **a** and the residuals from **b** and T_{mean} Apr-Sep temperatures; **d** Residuals between observed temperatures and the NegEx chronology (dark blue) and between observed temperatures and the combined chronology from **c** (turquoise)

for the sites used in the reconstruction to all available MXD datasets from *Abies* sites in Europe and Asia available through the ITRDB over their common period (1926–1975 CE), no significant difference is found ($p=0.34$; Fig. 7c). After performing pre-whitening of the NegEx chronology, the magnitude of the 1817 anomaly is slightly reduced compared to the standard chronology. However, 1817 remains a distinct negative anomaly (Fig. S18), suggesting that lag-1 autocorrelation alone cannot explain the 1817 anomaly and that independent climate forcing is required to explain its persistence after pre-whitening.

This interpretation is consistent with evidence for a different regional climate response to the Tambora eruption in the Central Himalayas. Historical documents indicate that China experienced below-average temperatures in 1816 but especially in 1817 CE, leading to severe crop damage and famines (Gao et al. 2017; Zhang et al. 1992). By contrast, there is little documentary evidence for large-scale cooling in India (Jameson 1820; Pant et al. 1992), though tree-ring evidence suggests 1816 CE as the driest year in India's western Himalayas in the past 300 years (Yadav et al. 2015). This extreme is potentially linked to different pressure systems from usual, caused by temperature anomalies due to the volcanic-induced cooling (Pfister & White 2018). On the Tibetan Plateau, Nie et al. (2023) identify both 1816 and 1817 CE as cold summers, with 1817 CE being one of the

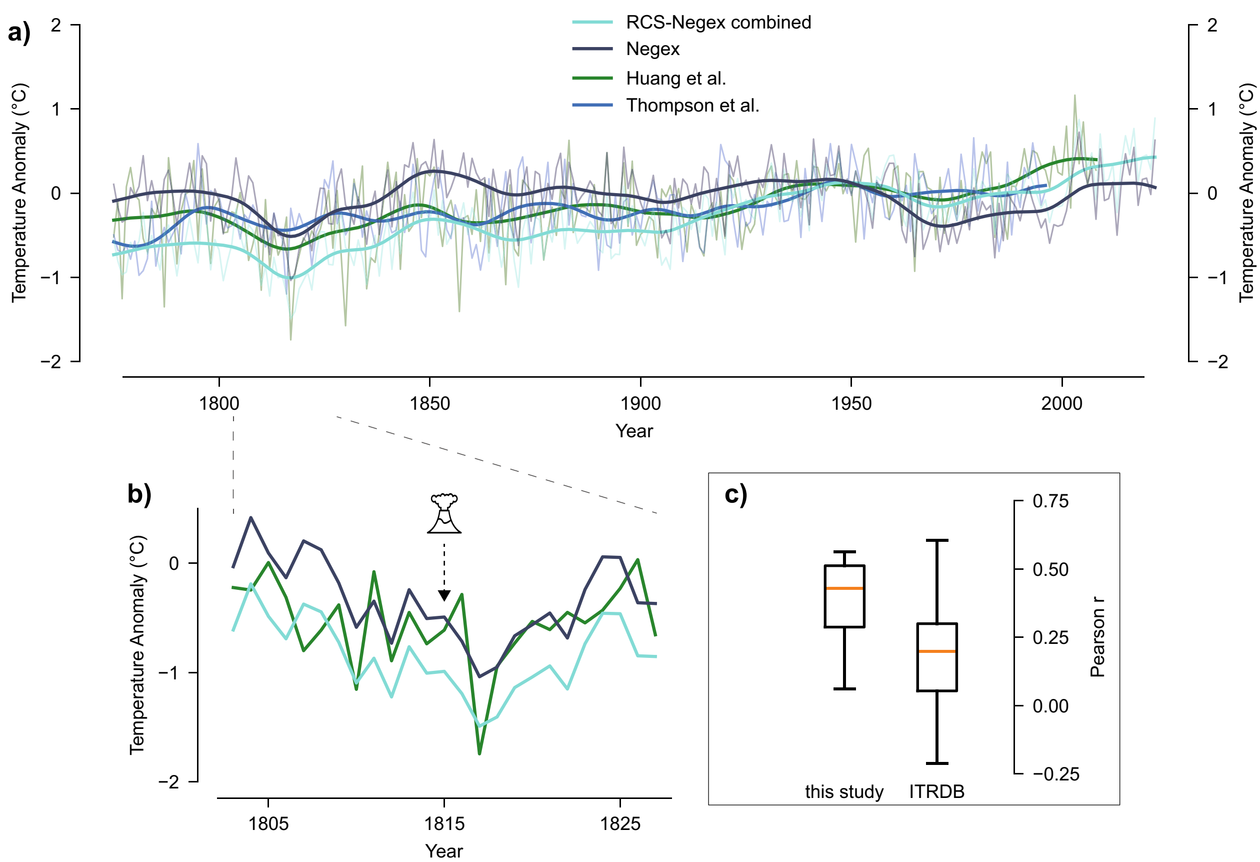

Fig. 7 **a** Comparison of proxy records (all scaled to 1900–1990 T_{mean} Apr-Sep, and smoothed using a 31-year gaussian filter): $\delta^{18}O$ based temperature reconstruction derived from a glacier (blue) (Thompson et al. 2000), MXD-based T_{min} reconstruction from the eastern TP (Huang et al. 2025) (green) and the chronologies introduced in this study (turquoise and dark blue); **b** Close-up view of the tree ring based proxy response to the 1815 CE Tambora eruption; **c** Lag-1 autocorrelation for the chronologies used in this study and all available *Abies* MXD-datasets from the ITRDB (common period 1926–1975 CE)

coldest in the past 1208 years. The MXD reconstructions by Wang et al. (2010) and Huang et al (2025; Fig. 7b) also display the year 1817 CE as cooler than 1816 CE, whereas the reconstruction by Li et al. (2017) outlines 1816 CE as the colder late summer-autumn compared to 1817 CE In Nepal-specific reconstructions, Cook et al. (2003) show 1817 CE February-June temperatures as also colder than 1816 CE, which is even surpassed by 1818 CE as the coldest year on record. This is similar to Cook et al. (2013), for which cooling continued until 1820 CE, and to a reconstruction by Gaire et al. (2020), who also found a cooling effect in the years following the eruption with a minimum in the early 1820s. Although some site chronologies display high autocorrelation, together with the evidence from other reconstructions and historic documents, the reconstruction presented here suggests that in the Nepalese Himalaya, the Tambora event did not lead to a single-year extreme in 1816 CE Instead, it is reasonable to assume that the eruption rather resulted in a multi-year cold anomaly spanning several subsequent years.

Conclusion

This study presents the first network-based MXD reconstruction of growing-season temperatures for the Central Himalayas, developed from four high-elevation *Abies spectabilis* sites. Temperature estimates extend back over 247 years and provide detailed insight into the climate variability of monsoon-influenced environments. The extended seasonality from April-September of the reconstruction reveals MXD as a valuable proxy for reconstructions during monsoonal conditions. Combining high- and low-frequency components from different detrending methods improves the agreement between proxy and instrumental data compared to classic NegEx approaches using only old trees. The reconstruction highlights a multi-year cold anomaly following the 1815 CE Tambora eruption, with the coldest summer being 1817 CE rather than 1816 CE This finding demonstrates the importance of regional reconstructions to improve understanding of climate response patterns to global cooling events. Expanding this network by adding species and sites across the Central Himalaya, as well as extending records back, is advised to gain further information on high-to-low frequency climate variability in these unique environments.

Acknowledgements Authors are grateful to the DNPWC-Nepal for research permission, and DHM for necessary hydro-climatic data, FRTC for providing dendro-laboratory facility. We express our sincere gratitude to the warden, officers, and staff of Rara and Langtang National Park for their kind cooperation during fieldwork.

Author contributions Conceptualization: TN, FR, JE; Fieldwork: TN, IKH, PR, ESK, SA, AB, NG; Data curation: TN; Formal Analysis: TN; Funding acquisition: JE; Investigation: TN, FR, MCAT, JE; Supervision: JE; Visualization: TN, FR; Writing—original draft: TN; Writing—review & editing: FR, MCAT, IKH, PR, ESK, MK, AK, SA, AB, NG, UB, JE.

Funding Open Access funding enabled and organized by Projekt DEAL. This work was supported by the German Research Foundation (Grant No. 514551733), the ERC Advanced Grant (# 882727; Monostar), the Czech Science Foundation grant HYDRO8 (23–08049S), TU-NPAR-079/80-ERG-12, the co-funded EU project AdAgriF (# CZ.02.01.01/00/22_008/0004635), and the ERC Synergy Grant (# 101118880; Synergy-Plague).

Declarations

Conflict of interest The authors declare that they have no known competing financial interests or personal relationships that could have appeared to influence the work reported in this paper.

References

Aryal S, Gaire NP, Pokhrel NR, Rana P, Sharma B, Kharal DK, Poudel BS, Dyola N, Fan ZX, Grießinger J, Bräuning A (2020) Spring season in western Nepal Himalaya is not yet warming: a 400-year temperature reconstruction based on tree-ring widths of Himalayan hemlock (*Tsuga dumosa*). Atmosphere 11(2):132. https://doi.org/10.3390/atmos11020132

Bhandari S, Gaire NP, Shah SK, Speer JH, Bhuju DR, Thapa UK (2019) A 307-year tree-ring spei reconstruction indicates modern drought in western Nepal Himalayas. Tree Ring Res 75(2):73. https://doi.org/10.3959/1536-1098-75.2.73

Björklund J, Seftigen K, Schweingruber F, Fonti P, von Arx G, Bryukhanova MV, Cuny HE, Carrer M, Castagneri D, Frank DC (2017) Cell size and wall dimensions drive distinct variability of earlywood and latewood density in Northern Hemisphere conifers. New Phytol 216(3):728–740. https://doi.org/10.1111/nph.14639

Björklund J, von Arx G, Nievergelt D, Wilson R, Van den Bulcke J, Günther B, Loader NJ, Rydval M, Fonti P, Scharnweber T, Andreu-Hayles L, Büntgen U, D'Arrigo R, Davi N, De Mil T, Esper J, Gärtner H, Geary J, Gunnarson BE, Hartl C, Hevia A, Song H, Janecka K, Kaczka RJ, Kirdyanov AV, Kochbeck M, Liu Y, Meko M, Mundo I, Nicolussi K, Oelkers R, Pichler T, Sánchez-Salguero R, Schneider L, Schweingruber F, Timonen M, Trouet V, Van Acker J, Verstege A, Villalba R, Wilmking M, Frank D (2019) Scientific merits and analytical challenges of tree-ring densitometry. Rev Geophys 57(4):1224–1264. https://doi.org/10.1029/2019rg000642

Bräuning A (2006) Tree-ring evidence of 'Little Ice Age' glacier advances in southern Tibet. Holocene 16(3):369–380. https://doi.org/10.1191/0959683606hl922rp

Bräuning A, Mantwill B (2004) Summer temperature and summer monsoon history on the Tibetan Plateau during the last 400 years recorded by tree rings. Geophys Res Lett 31(24):2004GL020793. https://doi.org/10.1029/2004gl020793

Bräuning A (2003) Tree-ring studies in the Dolpo-Himalya (western Nepal). Tree Rings in Archaeology, Climatology and Ecology (TRACE), 8–12

Briffa KR, Jones PD, Bartholin TS, Eckstein D, Schweingruber FH, Karlén W, Zetterberg P, Eronen M (1992a) Fennoscandian summers from ad 500: temperature changes on short and long timescales. Clim Dyn 7(3):111–119. https://doi.org/10.1007/BF00211153

Briffa KR, Jones PD, Schweingruber FH (1992b) Tree-ring density reconstructions of summer temperature patterns across western North America since 1600. J Clim 5(7):735–754

Büntgen U, Frank DC, Nievergelt D, Esper J (2006) Summer temperature variations in the European Alps, a.d. 755–2004. J Clim 19(21):5606–5623. https://doi.org/10.1175/jcli3917.1

Consortium PK (2013) Continental-scale temperature variability during the past two millennia. Nature Geosci 6(5):339–346. https://doi.org/10.1038/ngeo1797

Cook ER (1985) A Time Series Analysis Approach to Tree Ring Standardization: Bd. University of Arizona, PhD

Cook ER, Kairiukstis LA (1990) Methods of Dendrochronology: Applications in the Environmental Sciences. Springer

Cook ER, Krusic PJ (2020) Program ARSTAN: A tree-ring standardization program based on detrending and autoregressive time series modeling, with interactive graphics. Columbia University, Palisades, NY, Lamont-Doherty Earth Observatory

Cook ER, Briffa KR, Jones PD (1994) Spatial regression methods in dendroclimatology: a review and comparison of two techniques. Int J Climatol 14(4):379–402. https://doi.org/10.1002/joc.3370140404

Cook ER, Krusic PJ, Jones PD (2003) Dendroclimatic signals in long tree-ring chronologies from the Himalayas of Nepal. Int J Climatol 23(7):707–732. https://doi.org/10.1002/joc.911

Cook ER, Krusic PJ, Anchukaitis KJ, Buckley BM, Nakatsuka T, Sano M, Members PA (2013) Tree-ring reconstructed summer temperature anomalies for temperate East Asia since 800 C.E. Clim Dyn 41(11):2957–2972. https://doi.org/10.1007/s00382-012-1611-x

Cuny HE, Fonti P, Rathgeber CBK, von Arx G, Peters RL, Frank DC (2019) Couplings in cell differentiation kinetics mitigate air temperature influence on conifer wood anatomy. Plant Cell Environ 42(4):1222–1232. https://doi.org/10.1111/pce.13464

D'Arrigo R, Wilson R, Jacoby G (2006) On the long-term context for late twentieth century warming. J Geophys Res. https://doi.org/10.1029/2005jd006352

Department of Hydrology and Meteorology (DHM) (2017). Study of climate and climatic variation over Nepal. Department of Hydrology and Meteorology, Ministry of Science, Technology and Environment, Government of Nepal, Kathmandu, Nepal

Diffenbaugh NS, Giorgi F (2012) Climate change hotspots in the CMIP5 global climate model ensemble. Clim Change 114(3–4):813–822. https://doi.org/10.1007/s10584-012-0570-x

Duan AM, Xiao ZX (2015) Does the climate warming hiatus exist over the Tibetan Plateau? Sci Rep 5:13711. https://doi.org/10.1038/srep13711

Duan JP, Ma ZG, Li L, Zheng ZY (2019) August-September temperature variability on the Tibetan Plateau: past, present, and future. J Geophys Res Atmos 124(12):6057–6068. https://doi.org/10.1029/2019jd030444

Durbin J, Watson GS (1971) Testing for serial correlation in least squares regression. III. Biometrika 58(1):1. https://doi.org/10.2307/2334313

Dussaillant I, Hugonnet R, Huss M, Berthier E, Bannwart J, Paul F, Zemp M (2024). Annual mass changes for each glacier in the world from 1976 to 2023. https://doi.org/10.5194/essd-2024-323

Berkeley Earth (2025a). Global Gridded Data: Global Monthly Land . https://berkeleyearth.org/data/

Berkley Earth (2025b). Nepal. Temperature Region Page. Berkeley Earth. https://berkeleyearth.org/temperature-region/

Esper J, Cook ER, Schweingruber FH (2002) Low-frequency signals in long tree-ring chronologies for reconstructing past temperature variability. Science 295(5563):2250–2253. https://doi.org/10.1126/science.1066208

Esper J, Cook ER, Krusic PJ, Peters K, Schweingruber FH (2003) Tests of the RCS method for preserving low-frequency variability in long tree-ring chronologies. Tree-Ring Res 59(2):81–98

Esper J, Frank DC, Wilson RJS, Briffa KR (2005) Effect of scaling and regression on reconstructed temperature amplitude for the past millennium. Geophys Res Lett. https://doi.org/10.1029/2004gl021236

Esper J, Schneider L, Smerdon JE, Schöne BR, Büntgen U (2015) Signals and memory in tree-ring width and density data. Dendrochronologia 35:62–70. https://doi.org/10.1016/j.dendro.2015.07.001

Esper J, Reinig F, Torbenson M, del Castillo EM, Kunz M, Arzac A, Carrer M, Chen F, Kadioglu AK, Kirdyanov AV, Tejedor E, Trnka M, Büntgen U (2025) Pan-Alpine summer temperatures since 742 CE. Dendrochronologia 94:126432. https://doi.org/10.1016/j.dendro.2025.126432

Fan ZX, Bräuning A, Yang B, Cao KF (2009) Tree ring density-based summer temperature reconstruction for the central Hengduan Mountains in Southern China. Glob Planet Change 65(1–2):1–11. https://doi.org/10.1016/j.gloplacha.2008.10.001

Fisher RA (1921) On the probable error of a coefficient of correlation deduced from a small sample. Metron 1:3–32

Gaire NP, Bhuju DR, Koirala M, Shah SK, Carrer M, Timilsena R (2017) Tree-ring based spring precipitation reconstruction in western Nepal Himalaya since AD 1840. Dendrochronologia 42:21–30. https://doi.org/10.1016/j.dendro.2016.12.004

Gaire NP, Dhakal YR, Shah SK, Fan ZX, Bräuning A, Thapa UK, Bhandari S, Aryal S, Bhuju DR (2019) Drought (scPDSI) reconstruction of trans-Himalayan region of central Himalaya using *Pinus wallichiana* tree-rings. Palaeogeogr Palaeoclimatol Palaeoecol 514:251–264. https://doi.org/10.1016/j.palaeo.2018.10.026

Gaire NP, Fan ZX, Shah SK, Thapa UK, Rokaya MB (2020) Tree-ring record of winter temperature from Humla, Karnali, in central Himalaya: a 229 years-long perspective for recent warming trend. Geogr Ann Ser A Phys Geogr 102(3):297–316. https://doi.org/10.1080/04353676.2020.1751446

Gaire NP, Shah SK, Sharma B, Mehrotra N, Thapa UK, Fan ZX, Aryal PC, Bhuju DR (2023) Spatial minimum temperature reconstruction over the last three centuries for eastern Nepal Himalaya based on tree rings of *Larix griffithiana*. Theor Appl Climatol 152(1–2):895–910. https://doi.org/10.1007/s00704-023-04432-1

Gao CC, Gao YJ, Zhang Q, Shi CM (2017) Climatic aftermath of the 1815 Tambora eruption in China. J Meteor Res 31(1):28–38. https://doi.org/10.1007/s13351-017-6091-9

Guiterman CH, Gille E, Shepherd E, McNeill S, Payne CR, Morrill C (2024) The international tree-ring data bank at fifty: status of stewardship for future scientific discovery. Tree Ring Res. https://doi.org/10.3959/trr2023-2

Hamal K, Sharma S, Talchabhadel R, Ali M, Dhital YP, Xu TL, Dawadi B (2021) Trends in the diurnal temperature range over the southern slope of central Himalaya: retrospective and prospective evaluation. Atmosphere (Basel) 12(12):1683. https://doi.org/10.3390/atmos12121683

Hamed KH, Ramachandra Rao A (1998) A modified Mann-Kendall trend test for autocorrelated data. J Hydrol 204(1–4):182–196. https://doi.org/10.1016/S0022-1694(97)00125-X

Harington CR (1992) The Year without a summer? World climate in 1816. Canadian Museum of Nature

Hartl C, Schneider L, Riechelmann DFC, Kuhl E, Kochbeck M, Klippel L, Büntgen U, Esper J (2022) The temperature sensitivity along elevational gradients is more stable in maximum latewood density than tree-ring width. Dendrochronologia 73:125958. https://doi.org/10.1016/j.dendro.2022.125958

Holmes RL (1983) Computer-Assisted Quality Control in Tree-Ring Dating and Measurement. Tree Ring Bulletin 43:51–67

Homfeld IK, Büntgen U, Reinig F, Torbenson MCA, Esper J (2024) Application of RCS and signal-free RCS to tree-ring width and maximum latewood density data. Dendrochronologia 85:126205. https://doi.org/10.1016/j.dendro.2024.126205

Huang R, Yin H, Zhu HF, Liang EY, Ullah A, Jens-Henrik Meier W, Asad F, Bräuning A, Grießinger J (2025) A late summer temperature reconstruction based on tree-ring maximum latewood density since AD 1246 on the southeastern Tibetan Plateau. Quat Sci Rev 355:109266. https://doi.org/10.1016/j.quascirev.2025.109266

Hughes MK (2001) An improved reconstruction of summer temperature at Srinagar, Kashmir since AD 1660, based on tree-ring width and maximum latewood density of Abies pindrow [Royle] Spach. J Palaeosciences 50:13–19. https://doi.org/10.54991/jop.2001.1799

Hussain M, Mahmud I (2019) pyMannKendall: a Python package for non parametric Mann Kendall family of trend tests. J Open Source Softw 4(39):1556. https://doi.org/10.21105/joss.01556

ICIMOD (2023) Water, ice, society, and ecosystems in the Hindu Kush Himalaya:An outlook, edited by: Wester, P, Chaudhary, S, Chettri, N, Jackson, M, Maharjan, A, Nepal, S, and Steiner, JF, ICIMOD, Lalitpur, Nepal

Jameson J (1832) Art. XI. Report on the epidemic cholera Morbus, as it visited the Territories subject to the Presidency of Bengal, in the years 1817, 1818, and 1819. Am J Med Sci 9(18):441–487. https://doi.org/10.1097/00000441-183209180-00011

Khan A, Chen F, Saleem S, Chen YP, Zhang HL, Bakhtiyorov Z (2024) Tree-ring maximum latewood density reveals unprecedented warming and long-term summer temperature in the upper Indus Basin, northern Pakistan. Sci Total Environ 956:177393. https://doi.org/10.1016/j.scitotenv.2024.177393

Klippel L, Büntgen U, Konter O, Kyncl T, Esper J (2020) Climate sensitivity of high- and low-elevation *Larix decidua* MXD chronologies from the Tatra Mountains. Dendrochronologia 60:125674. https://doi.org/10.1016/j.dendro.2020.125674

Krishnan R, Shrestha AB, Ren GY, Rajbhandari R, Saeed S, Sanjay J, Abu Syed M, Vellore R, Xu Y, You QL, Ren YY (2019) Unravelling climate change in the Hindu Kush Himalaya: rapid warming in the mountains and increasing extremes. The Hindu Kush Himalaya assessment. Springer International Publishing, pp 57–97. https://doi.org/10.1007/978-3-319-92288-1_3

Krishnan R, Dhara C (2020) Executive Summary. In Assessment of Climate Change over the Indian Region, xii–xiix

Li MY, Wang L, Fan ZX, Shen CC (2015) Tree-ring density inferred late summer temperature variability over the past three centuries in the Gaoligong Mountains, southeastern Tibetan Plateau. Palaeogeogr Palaeoclimatol Palaeoecol 422:57–64. https://doi.org/10.1016/j.palaeo.2015.01.003

Li MQ, Huang L, Yin ZY, Shao XM (2017) Temperature reconstruction and volcanic eruption signal from tree-ring width and maximum latewood density over the past 304 years in the southeastern Tibetan Plateau. Int J Biometeorol 61(11):2021–2032. https://doi.org/10.1007/s00484-017-1395-0

Li MY, Duan JP, Wang L, Zhu HF (2018) Late summer temperature reconstruction based on tree-ring density for Sygera Mountain, southeastern Tibetan Plateau. Glob Planet Change 163:10–17. https://doi.org/10.1016/j.gloplacha.2018.02.005

Liang EY, Shao XM, Qin NS (2008) Tree-ring based summer temperature reconstruction for the source region of the Yangtze River on the Tibetan Plateau. Glob Planet Change 61(3–4):313–320. https://doi.org/10.1016/j.gloplacha.2007.10.008

Liang HX, Lyu LX, Wahab M (2016) A 382-year reconstruction of August mean minimum temperature from tree-ring maximum latewood density on the southeastern Tibetan Plateau, China. Dendrochronologia 37:1–8. https://doi.org/10.1016/j.dendro.2015.11.001

Lilliefors HW (1967) On the Kolmogorov-Smirnov test for normality with mean and variance unknown. J Am Stat Assoc 62(318):399–402

Liu J, Zhu G (2022) Geographical and geological GIS boundaries of the Tibetan Plateau and adjacent mountain regions (Version 2022.1). https://doi.org/10.5281/zenodo.6432940

Luterbacher J, Pfister C (2015) The year without a summer. Nature Geosci 8(4):246–248. https://doi.org/10.1038/ngeo2404

Nehrbass-Ahles C, Babst F, Klesse S, Nötzli M, Bouriaud O, Neukom R, Dobbertin M, Frank D (2014) The influence of sampling design on tree-ring-based quantification of forest growth. Glob Change Biol 20(9):2867–2885. https://doi.org/10.1111/gcb.12599

Nie Y, Pritchard HD, Liu Q, Hennig T, Wang WL, Wang XM, Liu SY, Nepal S, Samyn D, Hewitt K, Chen XQ (2021) Glacial change and hydrological implications in the Himalaya and Karakoram. Nat Rev Earth Environ 2(2):91–106. https://doi.org/10.1038/s43017-020-00124-w

Nie WZ, Li MQ, Deng GF, Shao XM (2023) Impacts of Atlantic multidecadal oscillation and volcanic forcing on the late summer temperature of the southern Tibetan Plateau. J Clim 36(20):7157–7177. https://doi.org/10.1175/jcli-d-22-0624.1

Olive DJ (2007) Prediction intervals for regression models. Comput Stat Data Anal 51(6):3115–3122. https://doi.org/10.1016/j.csda.2006.02.006

Oppenheimer C (2003) Climatic, environmental and human consequences of the largest known historic eruption: Tambora volcano (Indonesia) 1815. Prog Phys Geogr Earth Environ 27(2):230–259. https://doi.org/10.1191/0309133303pp379ra

Palazzi E, Filippi L, von Hardenberg J (2017) Insights into elevation-dependent warming in the Tibetan Plateau-Himalayas from CMIP5 model simulations. Clim Dyn 48(11):3991–4008. https://doi.org/10.1007/s00382-016-3316-z

Pant GB, Rupa Kumar K, Borgaonkar HP, Okada N, Fujiwara T, Yamashita K (2000) Climatic response of *Cedrus deodara* tree-ring parameters from two sites in the western Himalaya. Can J for Res 30(7):1127–1135. https://doi.org/10.1139/x00-038

Pant GB, Parthasarathy B, Sontakke NA (1992) Climate over India during the First Quarter of the Nineteenth Century. In The Year Without a Summer? World Climate in 1816 (S. 429–435). Canadian Museum of Nature

Panthi S, Bräuning A, Zhou ZK, Fan ZX (2017) Tree rings reveal recent intensified spring drought in the central Himalaya, Nepal. Glob Planet Change 157:26–34. https://doi.org/10.1016/j.gloplacha.2017.08.012

Pepin N, Bradley RS, Diaz HF, Baraer M, Caceres EB, Forsythe N, Fowler H, Greenwood G, Hashmi MZ, Liu XD, Miller JR, Ning L, Ohmura A, Palazzi E, Rangwala I, Schöner W, Severskiy I, Shahgedanova M, Wang MB, Williamson SN, Yang DQ (2015) Elevation-dependent warming in mountain regions of the world. Nat Clim Change 5(5):424–430. https://doi.org/10.1038/nclimate2563

Pfister C, White S (2018). A Year Without a Summer, 1816. In S. White, C. Pfister, & F. Mauelshagen (Hrsg.), The Palgrave Handbook of Climate History (S. 551–561). Palgrave Macmillan UK. https://doi.org/10.1057/978-1-137-43020-5_35

Qiu J (2008) China: the third pole. Nature 454(7203):393–396. https://doi.org/10.1038/454393a

Rathgeber CBK (2017) Conifer tree-ring density inter-annual variability–anatomical, physiological and environmental determinants. New Phytol 216(3):621–625. https://doi.org/10.1111/nph.14763

Ren YY, Ren GY, Sun XB, Shrestha AB, You QL, Zhan YJ, Rajbhandari R, Zhang PF, Wen KM (2017) Observed changes in surface air temperature and precipitation in the Hindu Kush Himalayan region over the last 100-plus years. Adv Clim Change Res 8(3):148–156. https://doi.org/10.1016/j.accre.2017.08.001

Rohde RA, Hausfather Z (2020) The Berkeley Earth Land/Ocean Temperature Record. Earth Syst Sci Data 12(4):3469–3479. https://doi.org/10.5194/essd-12-3469-2020

Sano M, Furuta F, Kobayashi O, Sweda T (2005) Temperature variations since the mid-18th century for western Nepal, as reconstructed from tree-ring width and density of *Abies spectabilis*. Dendrochronologia 23(2):83–92. https://doi.org/10.1016/j.dendro.2005.08.003

Schneider L, Smerdon JE, Büntgen U, Wilson RJS, Myglan VS, Kirdyanov AV, Esper J (2015) Revising midlatitude summer temperatures back to A.D. 600 based on a wood density network. Geophys Res Lett 42(11):4556–4562. https://doi.org/10.1002/2015gl063956

Schweingruber FH, Fritts HC, Bräker OU, Drew LG, Schär E (1978) The X-ray technique as applied to dendroclimatology. Tree-Ring Bull 38:61–91

Schweingruber FH (2002a) NOAA/WDS Paleoclimatology—Schweingruber—Ghorepanipass Annapurne—ABSB-ITRDB NEPA001 . NOAA National Centers for Environmental Information. https://doi.org/10.25921/3XCH-ZB08

Schweingruber FH (2002b) NOAA/WDS Paleoclimatology—Schweingruber—Kalingchok Gebirge—ABSB-ITRDB NEPA002 . NOAA National Centers for Environmental Information. https://doi.org/10.25921/JT3B-4C26

Shi F, Ge QS, Yang B, Li JP, Yang FM, Ljungqvist FC, Solomina O, Nakatsuka T, Wang NL, Zhao S, Xu CX, Fang KY, Sano M, Chu GQ, Fan ZX, Gaire NP, Zafar MU (2015) A multi-proxy reconstruction of spatial and temporal variations in Asian summer temperatures over the last millennium. Clim Change 131(4):663–676. https://doi.org/10.1007/s10584-015-1413-3

Shrestha AB, Wake CP, Mayewski PA, Dibb JE (1999) Maximum temperature trends in the Himalaya and its vicinity: an analysis based on temperature records from Nepal for the period 1971–94. J Climate 12(9):2775–2786. https://doi.org/10.1175/1520-0442(1999)012%3c2775:mttith%3e2.0.co;2

Sigdel SR, Zhang H, Zhu HF, Muhammad S, Liang EY (2020) Retreating glacier and advancing forest over the past 200 years in the central Himalayas. JGR Biogeosci. https://doi.org/10.1029/2020jg005751

Thakuri S, Dahal S, Shrestha D, Guyennon N, Romano E, Colombo N, Salerno F (2019) Elevation-dependent warming of maximum air temperature in Nepal during 1976–2015. Atmos Res 228:261–269. https://doi.org/10.1016/j.atmosres.2019.06.006

Thapa UK, Shah SK, Gaire NP, Bhuju DR (2015) Spring temperatures in the far-western Nepal Himalaya since AD 1640 reconstructed from *Picea smithiana* tree-ring widths. Clim Dyn 45(7):2069–2081. https://doi.org/10.1007/s00382-014-2457-1

Thompson LG, Yao T, Mosley-Thompson E, Davis ME, Henderson KA, Lin PN (2000) A high-resolution millennial record of the south Asian monsoon from Himalayan ice cores. Science 289(5486):1916–1919. https://doi.org/10.1126/science.289.5486.1916

Wang L, Duan JP, Chen J, Huang L, Shao XM (2010) Temperature reconstruction from tree-ring maximum density of Balfour spruce in eastern Tibet, China. Int J Climatol 30(7):972–979. https://doi.org/10.1002/joc.2000

Wang WC, Xiang Y, Gao Y, Lu AX, Yao TD (2015) Rapid expansion of glacial lakes caused by climate and glacier retreat in the Central Himalayas. Hydrol Process 29(6):859–874. https://doi.org/10.1002/hyp.10199

Wilson R, D'Arrigo R, Buckley B, Büntgen U, Esper J, Frank D, Luckman B, Payette S, Vose R, Youngblut D (2007) A matter of divergence: Tracking recent warming at hemispheric scales using tree ring data. J Geophys Res. https://doi.org/10.1029/2006jd008318

Wilson R, Anchukaitis K, Briffa KR, Büntgen U, Cook E, D'Arrigo R, Davi N, Esper J, Frank D, Gunnarson B, Hegerl G, Helama S, Klesse S, Krusic PJ, Linderholm HW, Myglan V, Osborn TJ, Rydval M, Schneider L, Schurer A, Wiles G, Zhang P, Zorita E (2016) Last millennium Northern Hemisphere summer temperatures from tree rings: Part I: The long term context. Quat Sci Rev 134:1–18. https://doi.org/10.1016/j.quascirev.2015.12.005

Xing P, Zhang QB, Lv LX (2014) Absence of late-summer warming trend over the past two and half centuries on the eastern Tibetan Plateau. Glob Planet Change 123:27–35. https://doi.org/10.1016/j.gloplacha.2014.10.006

Xu JC, Grumbine RE, Shrestha A, Eriksson M, Yang XF, Wang Y, Wilkes A (2009) The melting Himalayas: cascading effects of climate change on water, biodiversity, and livelihoods. Conserv Biol 23(3):520–530. https://doi.org/10.1111/j.1523-1739.2009.01237.x

Yadav RR, Misra KG, Yadava AK, Kotlia BS, Misra S (2015) Tree-ring footprints of drought variability in last ~300 years over Kumaun Himalaya, India and its relationship with crop productivity. Quat Sci Rev 117:113–123. https://doi.org/10.1016/j.quascirev.2015.04.003

Yu H, Hutson AD (2024) A robust Spearman correlation coefficient permutation test. Commun Stat Theory Meth 53(6):2141–2153. https://doi.org/10.1080/03610926.2022.2121144

Zhang PY, Wang WC, Hameed S (1992) Evidence for Anomalous Cold Weather in China 1815−1817. In: World climate in 1816. The year without the summer? Canadian Museum of Nature